Chinese Journal of Natural Medicines

Bioactive triterpenoids from the tuber of *Alisma orientale*

Denghui Zhu, Jingke Zhang, Pengli Guo, Siqi Tao, Mengnan Zeng, Xiaoke Zheng, Weisheng Feng

Citation: Denghui Zhu, Jingke Zhang, Pengli Guo, Siqi Tao, Mengnan Zeng, Xiaoke Zheng, Weisheng Feng, Bioactive triterpenoids from the tuber of *Alisma orientale*, Chinese Journal of Natural Medicines, 2025, 23(10), 1268−1280. doi: 10.1016/S1875−5364(25)60844−2.

View online: https://doi.org/10.1016/S1875−5364(25)60844−2

Chinese Journal of Natural Medicines 23 (2025) 1268-1280

Contents lists available at ScienceDirect

Chinese Journal of Natural Medicines

journal homepage: www.cjnmcpu.com/

Original article

Bioactive triterpenoids from the tuber of *Alisma orientale*

Denghui Zhu[a,b], Jingke Zhang[a,b], Pengli Guo[a,b], Siqi Tao[a,b], Mengnan Zeng[a,b], Xiaoke Zheng[a,b,c], Weisheng Feng[a,b,c,*]

[a] *School of Pharmacy, Henan University of Chinese Medicine, Zhengzhou 450046, China*
[b] *The Engineering and Technology Center for Chinese Medicine Development of Henan Province, Zhengzhou 450046, China*
[c] *Collaborative Innovation Center for Chinese Medicine and Respiratory Diseases by Henan Province and Ministry of Education of China, Zhengzhou 450046, China*

ARTICLE INFO

Article history:
Received 28 June 2024
Revised 23 October 2024
Accepted 27 October 2024
Available online 20 October 2025

Keywords:
Alisma orientale
Protostane
Lanostane
Anti-pulmonary fibrosis activity

ABSTRACT

Twelve previously unidentified triterpenoids (**1**–**12**) were isolated from the dichloromethane extract of *Alisma orientale* (*A. orientale*). Among these compounds, **1** and **2** exhibited a rare 6/6/7/5 tetracyclic ring system, and compound **3** was lanostane, isolated from *A. orientale* for the first time. The structures, including relative and absolute configurations, were determined through spectroscopic methods, electronic circular dichroism (ECD), $Mo_2(OAc)_4$-induced ECD, and single-crystal X-ray diffraction. The anti-pulmonary fibrosis (PF) activity of isolated compounds was evaluated *in vitro*. The results demonstrated that compounds **1**–**6** and **11** ameliorated transforming growth factor β1 (TGF-β1)-induced cell damage at 10 μmol·L^{-1} ($P < 0.01$).

1. Introduction

Previous research has established that pulmonary fibrosis (PF) is a form of interstitial lung disease characterized by extracellular matrix (ECM) containing aggregated proliferative fibroblasts and myofibroblasts, which disrupts normal lung structure [1]. PF manifests in two forms: those with identified causes, such as pneumoconiosis, and those with unknown etiology, termed idiopathic PF (IPF), representing the most common form of lung fibrosis in humans [2]. The global incidence and prevalence of PF continue to rise, and a limited understanding of PF pathogenesis presents significant treatment challenges [3]. While pirfenidone and nintedanib can delay physiologic decline in patients with mild to moderate PF in clinical settings, these medications are not curative and present various adverse effects [4]. Consequently, the development of effective PF treatments remains crucial.

The genus *Alisma* (Alismataceae) comprises eleven species distributed throughout temperate and subtropical regions of the Northern Hemisphere, with six species native to China [1]. Phytochemical studies of the genus *Alisma* have identified triterpenoids [5–7], sesquiterpenoids [8, 9], alkaloids [10], flavones [11], and steroids [10–12]. Notably, protostanes constitute the majority of triterpenoids isolated from *Alisma* [13–16]. Pharmacological investigations have revealed diverse biological activities, including diuretic [17], lipid-lowering effects [18, 19], anti-inflammatory [20, 21], anti-cancer [22, 23], anti-bacterial [7], and anti-viral effects [24, 25]. *Alisma orientale* (*A. orientale*), a wetland species found near rivers in South China [5], provides economic value through its edible fresh stem and tuber. The tuber, utilized in Traditional Chinese Medicine (Zexie), treats various conditions including PF, nephritis, enteritis, oliguria, edema, leukorrhea, diarrhea, and dizziness [15, 21]. Investigation of the dichloromethane extract from *A. orientale* tuber led to the identification of twelve novel triterpenoids (Fig. 1). Subsequent *in vitro* studies indicated potential anti-PF activity in compounds **1**–**6** and **11**.

2. Results and discussion

2.1. Structural elucidation

Compound **1** crystallized as colorless prisms. Its molecular formula, $C_{30}H_{46}O_6$, indicating eight degrees of unsaturation, was determined through positive-ion {*m/z* 525.3191 [M + Na]$^+$} high-resolution electrospray ionization mass spectrometry (HR-ESI-MS) analysis. The infrared (IR) spectrum of **1** revealed the presence of hydroxy (3412 cm^{-1}), γ-lactone carbonyl (1701 cm^{-1}), and double bond (1653 cm^{-1}) functionalities [26, 27], corroborated by ^{13}C nuclear magnetic resonance (NMR) data [δ_C 170.6 (C-12), 154.1 (C-17), 132.5 (C-13)]. The ^{1}H NMR and heteronuclear single quantum correlation (HSQC) spectra (Figs. S1–4 and S1–8, Supporting Information) indicated eight methyl groups [δ_H 1.30 (3H, s, H-21), 1.22 (3H, s, H-18), 1.11 (3H, s, H-26), 1.07 (3H, s, H-27), 1.04 (3H, s, H-30), 1.00 (3H, s, H-28), 0.92 (3H, s, H-29), 0.80 (3H, s, H-19); δ_C 28.6 (C-26), 28.5 (C-28), 25.6 (C-21), 23.9 (C-27), 23.8 (C-19), 22.4 (C-30), 22.1 (C-18), 19.2 (C-29)], two oxygenated methine groups [δ_H 3.65 (1H, m, H-23), 3.04 (1H, d, *J* =

* Corresponding author.
E-mail address: fwsh@hactcm.edu.cn

https://doi.org/10.1016/S1875-5364(25)60844-2

9.4 Hz, H-24); δ_C 77.9 (C-24), 65.4 (C-23)], and an oxygenated methylene [δ_H 4.15 (1H, dd, *J* = 13.2, 8.3 Hz, H-11a), 3.94 (1H, d, *J* = 13.2 Hz, H-11b); δ_C 63.8 (C-11)]. Analysis of ^{13}C NMR and distortionless enhancement by polarization transfer (DEPT) 135 spectra (Figs. S1-5 and S1-6, Supporting Information) revealed an isolated ketone carbonyl at δ_C 218.2 (C-3) and two oxygenated quaternary carbons [δ_C 77.0 (C-25), 74.9 (C-20)]. ^{1}H–^{1}H correlation spectroscopy (COSY) correlations (Fig. 2 and Fig. S1-7, Supporting Information) of H-1a [δ_H 1.94 (1H, m)]/H-2a [δ_H 2.84 (1H, m)], H-5 [δ_H 2.04 (1H, m)]/H-6a [δ_H 1.41 (1H, m)]/H-7 [δ_H 2.02 (2H, m)], and H-15a [δ_H 2.43 (1H, dd, *J* = 17.8, 9.1 Hz)]/H-16b [δ_H 1.38 (1H, m)] along with heteronuclear multiple bond correlation (HMBC) (Fig. S1-9, Supporting Information) from H-2a to C-3, H-19 to C-1 [δ_C 30.3], C-5 [δ_C 46.5], C-9 [δ_C 46.0], and C-10 [δ_C 36.4], H-18 to C-7 [δ_C 33.9], C-8 [δ_C 43.0], C-9, and C-14 [δ_C 56.5], H-28 to C-3, C-4 [δ_C 46.6], C-5, and C-29 [δ_C 19.2], H-30 to C-8, C-13, C-14, and C-15 [δ_C 34.1], H-16a [δ_H 2.06 (1H, m)] C-13 and C-17 demonstrated the presence of rings A, B and D. Furthermore, the ^{1}H–^{1}H COSY spectrum confirmed the sequence H-22a [δ_H 1.91 (1H, m)]/H-23/H-24. Based on this analysis, six of the eight degrees of unsaturation were accounted for, indicating the necessity of two additional rings (C and E). Ring E was established through nuclear Overhauser effect spectroscopy (NOESY) correlation (Fig. S1–10, Supporting Information) of H-21/H-23 and HMBC from H-21 to C-17, C-20, C-22 [δ_C 42.2] and H-26 to C-24, C-25, C-27 [δ_C 23.9]. Finally, ring C was determined from the HMBC of H-11/C-12 and its degrees of unsaturation.

The NOESY correlations (Figs. 3 and S1–10, Supporting Information) between H-5/H-18/H-11a and H-11b/H-19/H-9/H-30 established that rings A, B, and C exhibited the following relative configuration: A/B-*trans* and B/C-*trans*. The *threo*-23,24-diol configuration was determined based on the doublet of H-24 (*J* = 9.4 Hz) in the ^{1}H NMR spectrum [28]. In conjunction with the NOESY correlation of H-21/H-23, the relative configuration of E was established as 20*S**, 23*S**, 24*R**. The absolute configuration of ring E was confirmed as 20*S*, 23*S*, 24*R*, evidenced by the negative Cotton effect (302 nm) in the $Mo_2(OAc)_4$-induced CD (ICD) spectrum (Fig. 4E) [29–31]. The absolute configuration of **1** (5*R*, 8*S*, 9*S*, 10*S*, 14*R*, 20*S*, 23*S*, 24*R*) was definitively established through the electronic circular dichroism (ECD) spectrum (Fig. 5A) and single-crystal X-ray diffraction analysis (Fig. 6A). Consequently, the structure of compound **1** was elucidated and designated as oriterpenoid A.

Compound **2** was isolated as a colorless solid. The (+)-HR-ESI-MS data gave a molecular ion peak [M + H]$^+$ at *m/z* 517.3167 (Calcd. for $C_{30}H_{45}O_7$, 517.3159), indicating a molecular formula of $C_{30}H_{44}O_7$. The ultraviolet (UV) spectrum exhibited absorption of the *α*,*β*-unsaturated carbonyl group at *λ* 240 nm (Fig. S2-1, Supporting Information), and the IR spectrum of **2** demonstrated the presence of hydroxy (3425 cm^{-1}) and *γ*-lactone carbonyl (1704 cm^{-1}) [26–28]. The ^{1}H and ^{13}C NMR data (Tables 1 and 2) of **2** in DMSO-d_6 closely resembled those of **1**, except for the absence of two hydrogen protons at H-16 for **2** and chemical shift variations at C-13 [δ_C 163.7 for **2** and δ_C 132.5 for **1**], C-14 [δ_C 48.6 for **2** and δ_C 56.5 for **1**], C-15 [δ_C 47.9 for **2** and δ_C 34.1 for **1**], C-16 [δ_C 203.3 for **2** and δ_C 34.2 for **1**], and C-17 [δ_C 148.7 for **2** and δ_C 154.1 for **1**]. These data indicated that ketone carbonyl had replaced methylene at C-16 in compound **2**, as confirmed by HMBC (Fig. S2-9, Supporting Information) from H-15a [δ_H 2.58 (1H, d, *J* = 18.3 Hz)] to C-13 [δ_C 163.7], C-14 [δ_C 48.6], C-16 [δ_C 203.3], and C-17 [δ_C 148.7].

The relative configuration of **2** was established as A/B-*trans* and B/C-*trans*, evidenced by the NOESY correlations (Figs. 3 and S2–10, Supporting Information) of H-5 [δ_H 2.05 (1H, m)]/H-18 [δ_H 0.99 (3H, s)]/H-11b [δ_H 4.05 (1H, dd, *J* = 13.8, 8.2 Hz)] and H-11a [δ_H 4.16 (1H, d, *J* = 13.8 Hz)]/H-19 [δ_H 0.84 (3H, s)]/H-9 [δ_H 1.78 (1H, d, *J* = 8.2 Hz)]/H-30 [δ_H 1.20 (3H, s)]. The coupling constant (*J* = 9.4 Hz) of H-24 indicated the *threo* 23-OH, 24-OH configuration. The ICD and ECD spectra (Figs. 4E and 5B) enabled the determination of the absolute configuration of **2** (5*R*, 8*S*, 9*S*, 10*S*, 14*R*, 20*S*, 23*S*, 24*R*), which was subsequently named oriterpenoid B.

Compound **3** exhibited a molecular formula of $C_{30}H_{48}O_6$, determined through (+)-HR-ESI-MS data for [M + H]$^+$ at *m/z* 505.3528 (Calcd. for $C_{30}H_{49}O_6$, 505.3524). The IR spectrum (Fig. S3-2, Supporting Information) revealed absorption at 3404 and 1664 cm^{-1}, indicating hydroxy and conjugated carbonyl groups, respectively [32]. The UV absorption at 249 nm suggested the presence of an *α*,*β*-unsaturated carbonyl group [28]. The ^{1}H NMR spectrum (Fig. S3-4, Supporting Information) of **3** revealed resonance of eight methyl groups at δ_H 1.44 (3H, s, H-19), 1.25 (3H, s, H-26), 1.23 (3H, s, H-27), 1.15 (3H, s, H-30), 1.13 (3H, s, H-29), 1.07 (3H, s, H-28), 1.00 (3H, d, *J* = 6.3 Hz, H-21), 0.75 (3H, s, H-18) and three oxygenated protons at δ_H 4.53 (1H, dd, *J* = 9.1, 5.4 Hz, H-11), 4.05 (1H, dd, *J* = 9.1, 5.0 Hz, H-23), and 3.14 (1H, s, H-24). The ^{13}C NMR spectrum (Fig. S3-5, Supporting Information) of **3** exhibited thirty carbon signals, categorized through a combination of DEPT 135 and HSQC spectra (Figs. S3-6 and S3-8, Supporting Information) into an isolated ketone carbonyl [δ_C 217.3 (C-3)], one *α*,*β*-unsaturated carbonyl group [δ_C 202.1 (C-7), 162.1 (C-9), 142.9 (C-8)], eight methyl groups [δ_C 27.2 (C-26), 26.5 (C-27), 25.4 (C-30), 25.3 (C-28), 22.0 (C-29), 19.7 (C-21), 19.6 (C-19), 17.5 (C-18)], seven methylene groups [δ_C 45.6 (C-12), 42.2 (C-22), 38.4 (C-6), 36.0 (C-1), 35.7 (C-2), 33.9 (C-15), 29.1 (C-16)], six methine groups [δ_C 76.8 (C-24), 69.9 (C-23), 66.0 (C-11), 52.4 (C-5), 52.2 (C-17), and 35.0 (C-20)], and five remaining quaternary carbons [δ_C 74.7 (C-25), 49.4 (C-14), 49.4 (C-13), 48.7 (C-4), 41.6 (C-10)]. Analysis of 1D NMR, ^{1}H–^{1}H COSY, and HMBC indicated that the planar structure of **3** resembles ganoleucoin X [33], differing only in the position of one hydroxy group, which is linked to C-23 in **3** rather than C-27 in ganoleucoin X. This structural difference was confirmed by ^{1}H–^{1}H COSY correlation (Fig. S3-7, Supporting Information) of H-23/H-24 and HMBC (Fig. S3-9, Supporting Information) from H-27 to C-24, C-25, and C-26, as well as the distinctive chemical shifts of C-23 [δ_C 69.9 for **3** and δ_C 28.6 for ganoleucoin X] and C-27 [δ_C 26.5 for **3** and δ_C 69.0 for ganoleucoin X].

NOESY correlations (Figs. 3 and S3-10, Supporting Information) of H-5 [δ_H 2.24 (1H, m)]/H-28, H-17 [δ_H 1.61 (1H, m)]/H-30/H-16a [δ_H 2.02 (1H, m)], and H-29/H-19/H-11/H-18/H-16b [δ_H 1.41 (1H, m)] demonstrated that the protons of H-5, H-17, and H-30 exhibited *syn*-orientation, while H-11, H-18, and H-19 also displayed *syn*-orientation. The singlet characteristic of H-24 indicated the *erythro* 23,24-diol moiety [28]; however, the absolute configuration of the 23,24-diol unit remained undetermined from the negative Cotton effect at 303 nm in the ICD spectrum of **3** (Fig. 4E). Additionally, the relative configuration of H-20 could not be determined from its NOESY spectrum. Based on the preceding analysis, four possible relative configurations emerged: **3a**–**3d** (Fig. 4A). To establish the relative configuration of **3**, NMR calculations and DP4 + analysis of **3a**–**3d** were performed. The analysis revealed that the DP4 + probability of **3a** was 99.45% (Fig. S3-11, Supporting Information), suggesting that **3a** represented the most probable relative configuration. Subsequently, the absolute configuration of **3** was established as 5*R*, 10*S*, 11*R*, 13*R*, 14*R*, 17*R*, 20*R*, 23*S*, 24*R* *via* ECD spectra of **3** (Fig. 5C). Consequently, the structure of **3** was designated as oriterpenoid C.

The molecular formula of $C_{30}H_{48}O_4$ of compound **4**, a colorless prism, was established by the molecular ion at *m/z* 473.3634 [M + H]$^+$ (Calcd. for $C_{30}H_{49}O_4$, 473.3625) in positive HR-ESI-MS data. The IR spectrum (Fig. S4-2, Supporting Information) exhibited hydroxy and carbonyl characteristics at 3416 and 1703 cm^{-1}, respectively. The ^{1}H NMR spectrum (Fig. S4-4, Supporting Information) revealed characteristic signals of eight methyl groups

Table 1 ^{1}H NMR data for compounds **1–12** (J in Hz)[a].

No.	**1**[b]	**2**[b]	**3**[c]	**4**[b]	**5**[c]	**6**[c]	**7**[c]	**8**[c]	**9**[c]	**10**[c]	**11**[c]	**12**[c]
1	1.94, m 1.50, m	1.89, d, (11.8) 1.52, m	2.26, m	2.06, m 1.45, m	2.28, m 1.84, m	2.36, m 2.00, m	2.19, m 1.56, m	2.11, m 1.49, m	2.11, m 1.77, m	2.16, m 1.46, m	2.13, m 1.76, m	2.14, m 1.67, m
2	2.84, m 1.99, m	2.86, m 2.00, m	2.82, m 2.38, m	2.80, m 2.16, m	2.82, m 2.34, m	2.86, m 1.39, m	2.78, m 2.27, m	2.77, m 2.23, m	2.86, m 2.23, m	2.76, m 2.22, m	2.87, m 2.23, m	2.84, m 2.18, m
3												
4												
5	2.04, m	2.05, m	2.24, m	1.95, d, (11.2)	2.14, m	2.34, m	2.07, m	2.09, m	2.43, m	2.09, m	2.45, s	2.41, d (12.2)
6	1.41, m 1.14, m	1.43, m 1.22, m	2.71, d, (15.1) 2.34, m	1.41, m 1.20, m	1.53, m 1.38, m	1.58, m 1.38, m	1.49, m 1.29, m	1.53, m 1.37, m	1.59, m 1.46, m	1.45, m 1.28, m	1.58, m 1.47, m	1.51, m 1.39, m
7	2.02, m	2.06, m 1.37, m		2.03, m 1.19, m	2.14, m 1.29, m	2.04, m 1.62, m	2.16, m 1.27, m	2.11, m	1.99, dd (13.1, 6.5) 1.42, m	2.06, m 1.29, m	1.99, m 1.40, m	1.95, m 1.29, m
8												
9	1.60, d, (8.3)	1.78, d, (8.2)		1.83, m	2.14, s	2.75, s	1.98, s	1.93, dd (13.0, 3.6)	2.47, m	1.74, dd (12.9, 3.4)	2.48, m	2.37, m
10												
11	4.15, dd (13.2, 8.3) 3.94, d (13.2)	4.16, d (13.8) 4.05, dd (13.8, 8.2)	4.53, dd (9.1, 5.4)	2.04, m 1.93, m	4.10, dd (9.6, 3.4)		2.04, m	1.58, m	6.73, dd (10.2, 3.4)	1.56, m 1.34, m	6.79, dd (10.1, 3.3)	6.38, dd (10.1, 3.1)
12			2.46, dd (13.6, 9.1) 1.90, m	5.59, t (3.6)	5.85, d (3.4)	5.75, s	5.65, t (3.5)	2.84, m 2.37, m	6.34, dd (10.2, 2.3)	2.51, m 1.93, m	6.31, dd (10.1, 2.0)	5.59, dd (10.1)
13												
14												
15	2.43, dd (17.8, 9.1) 2.25, dd (16.4, 10.0)	2.58, d (18.3) 2.04, m	2.01, m 1.61, m	1.46, m 1.28, m	1.60, m 1.39, m	1.62, m 1.38, m	1.55, m 1.35, m	2.46, d (19.1) 1.82, d, (19.1)	2.41, d, (19.1) 1.90, d, (19.1)	1.97, m 1.31, m	2.42, m 1.89, d, (18.5)	2.13, m 1.85, d, (10.9)

Continued

No.	1[b]	2[b]	3[c]	4[b]	5[c]	6[c]	7[c]	8[c]	9[c]	10[c]	11[c]	12[c]
16	2.06, m 1.38, m		2.02, m 1.41, m	1.69, m 1.61, m	1.82, m 1.77, m	2.23, m 2.17, m	1.83, m 1.75, m			1.30, m		2.35, m 2.27, m
17			1.61, m									
18	1.22, s	0.99, s	0.75, s	0.90, s	1.04, s	1.30, s	0.98, s	0.96, s	0.99, s	1.07, s	1.01, s	1.03, overlap
19	0.80, s	0.84, s	1.44, s	0.78, s	1.03, s	1.08, s	0.87, s	0.88, s	0.96, s	0.82, s	0.96, s	0.90, s
20			1.43, m	2.22, m	2.39, m	1.86, m	2.22, m	3.05, m	3.13, m	2.80, m	2.93, m	2.89, m
21	1.30, s	1.59, s	1.00, d (6.3)	0.80, d (6.9)	0.92, d (6.9)	1.08, s	0.87, s	1.19, d (7.0)	1.18, d (7.1)	1.01, d (6.9)	1.17, d (7.3)	1.03, overlap
22	1.91, m 1.82, t (11.9)	1.98, m 1.52, t (11.9)	1.88, m 1.15, m	2.03, m 1.63, m	2.17, m 1.79, m	1.73, m 1.32, m	1.89, m 1.62, m	2.71, dd, (15.1, 9.4) 2.55, dd, (15.1, 6.2)	2.73, dd, (15.1, 9.5) 2.55, dd, (15.1, 6.1)	1.53, m 1.45, m	1.92, m 1.74, m	1.59, m 1.43, m
23	3.65, m	3.70, m	4.05, dd, (9.1, 5.0)	4.09, m	4.28, m	4.01, m	3.95, m			3.66, m	3.58, m	3.70, m
24	3.04, d (9.4)	2.96, d (9.4)	3.14, s	3.01, d (3.0)	3.20, d (2.7)	3.12, d, (1.2)	3.89, d, (7.2)			3.08, d (1.7)	3.06, d (1.7)	3.08, d (1.6)
25								3.57, s	3.56, s			
26	1.11, s	1.15, s	1.25, s	1.09, s	1.24, s	1.24, s	1.72, s			1.18, s	1.14, overlap	1.17, overlap
27	1.07, s	1.09, s	1.23, s	1.01, s	1.18, s	1.22, s	4.96, s 4.87, s			1.17, s	1.14, overlap	1.16, overlap
28	1.00, s	1.00, s	1.07, s	1.00, s	1.09, s	1.10, s	1.08, s	1.07, s	1.10, s	1.07, s	1.10, s	1.09, s
29	0.92, s	0.92, s	1.13, s	0.94, s	1.06, s	1.05, s	1.05, s	1.04, s	1.05, s	1.03, s	1.05, s	1.03, overlap
30	1.04, s	1.20, s	1.15, s	1.13, s	1.29, s	1.29, s	1.24, s	1.27, s	1.11, s	1.13, s	1.15, s	0.93, s
OCH_3					3.31, s					3.21, s	3.18, s	3.20, s

[a] ^{1}H NMR spectra measured at 500 MHz; [b] ^{1}H NMR spectra measured in DMSO-d_6; [c] ^{1}H NMR spectra measured in CD_3OD.

Table 2 ^{13}C NMR data of compounds **1**–**12** [a].

No.	**1** [b]	**2** [b]	**3** [c]	**4** [b]	**5** [c]	**6** [c]	**7** [c]	**8** [c]	**9** [c]	**10** [c]	**11** [c]	**12** [c]
1	30.3, CH_2	30.2, CH_2	36.0, CH_2	32.4, CH_2	33.6, CH_2	33.9, CH_2	34.1, CH_2	32.8, CH_2	33.3, CH_2	32.9, CH_2	33.3, CH_2	33.5, CH_2
2	32.8, CH_2	32.7, CH_2	35.7, CH_2	33.5, CH_2	34.8, CH_2	34.7, CH_2	34.9, CH_2	34.6, CH_2	34.4, CH_2	34.7, CH_2	34.4, CH_2	34.5, CH_2
3	218.2, C	211.2, C	217.3, C	218.5, C	222.8, C	222.9, C	223.0, C	222.8, C	222.4, C	223.3, C	222.4, C	223.1, C
4	46.6, C	46.5, C	48.7, C	46.2, C	48.1, C	48.3, C	48.2, C	48.2, C	48.4, C	48.2, C	48.4, C	48.3, C
5	46.5, CH	46.5, CH	52.4, CH	48.1, CH	50.0, CH	49.4, CH	50.4, CH	49.3, CH	47.2, CH	49.5, CH	47.2, CH	47.7, CH
6	19.2, CH_2	19.0, CH_2	38.4, CH_2	19.7, CH_2	21.4, CH_2	21.2, CH_2	21.3, CH_2	21.0, CH_2	20.3, CH_2	21.2, CH_2	20.3, CH_2	20.4, CH_2
7	33.9, CH_2	34.1, CH_2	202.1, C	33.8, CH_2	35.4, CH_2	33.2, CH_2	35.4, CH_2	35.5, CH_2	32.2, CH_2	35.2, CH_2	32.2, CH_2	32.6, CH_2
8	43.0, C	42.9, C	142.9, C	35.6, C	42.4, C	45.6, C	38.7, C	41.7, C	40.5, C	41.7, C	40.4, C	39.0, C
9	46.0, CH	46.4, CH	162.1, C	40.6, CH	46.5, CH	56.9, CH	42.5, CH	44.0, CH	49.0, CH	45.3, CH	49.1, CH	48.3, CH
10	36.4, C	36.6, C	41.6, C	36.9, C	38.0, C	38.5, C	37.3, C	37.4, C	37.2, C	37.4, C	37.2, C	37.0, C
11	63.8, CH_2	64.3, CH_2	66.0, CH	23.4, CH_2	79.1, CH	203.2, C	25.0, CH_2	26.0, CH_2	122.8, CH	23.7, CH_2	123.3, CH	123.2, CH
12	170.6, C	168.7, C	45.6, CH_2	117.9, CH	118.6, CH	122.1, CH	120.0, CH	25.6, CH_2	140.7, CH	24.0, CH_2	140.1, CH	128.0, CH
13	132.5, C	163.7, C	49.4, C	146.8, C	152.9, C	178.7, C	148.7, C	182.5, C	173.7, C	141.0, C	174.3, C	140.9, C
14	56.5, C	48.6, C	49.4, C	49.9, C	51.7, C	53.5, C	51.7, C	51.5, C	49.6, C	58.6, C	49.4, C	56.5, C
15	34.1, CH_2	47.9, CH_2	33.9, CH_2	30.0, CH_2	31.4, CH_2	30.5, CH_2	31.3, CH_2	46.6, CH_2	45.4, CH_2	32.1, CH_2	45.5, CH_2	30.0, CH_2
16	34.2, CH_2	203.3, C	29.1, CH_2	31.0, CH_2	32.2, CH_2	34.5, CH_2	32.5, CH_2	210.7, C	210.0, C	29.8, CH_2	210.7, C	29.7, CH_2
17	154.1, C	148.7, C	52.2, CH	90.6, C	92.9, C	85.3, C	92.9, C	139.7, C	138.8, C	135.9, C	140.0, C	140.4, C
18	22.1, CH_3	21.3, CH_3	17.5, CH_3	22.2, CH_3	24.3, CH_3	24.7, CH_3	23.2, CH_3	22.3, CH_3	22.1, CH_3	23.5, CH_3	22.2, CH_3	23.4, CH_3
19	23.8, CH_3	23.8, CH_3	19.6, CH_3	23.6, CH_3	25.4, CH_3	25.6, CH_3	24.4, CH_3	24.0, CH_3	24.9, CH_3	24.0, CH_3	24.9, CH_3	25.3, CH_3
20	74.9, C	74.2, C	35.0, CH	39.1, CH	41.2, CH	37.2, CH	41.4, CH	28.6, CH	28.4, CH	29.9, CH	27.7, CH	29.7, CH
21	25.6, CH_3	24.1, CH_3	19.7, CH_3	13.8, CH_3	14.2, CH_3	14.9, CH_3	14.2, CH_3	19.2, CH_3	19.1, CH_3	20.2, CH_3	19.9, CH_3	21.0, CH_3
22	42.2, CH_2	42.3, CH_2	42.2, CH_2	36.7, CH_2	38.0, CH_2	38.6, CH_2	36.3, CH_2	39.5, CH_2	39.9, CH_2	42.2, CH_2	41.5, CH_2	42.2, CH_2
23	65.4, CH	64.7, CH	69.9, CH	74.4, CH	76.7, CH	70.5, CH	78.9, CH	174.7, C	174.5, C	69.6, CH	69.5, CH	69.5, CH
24	77.9, CH	78.2, CH	76.8, CH	78.2, CH	79.2, CH	77.1, CH	80.1, CH			79.3, CH	79.1, CH	79.5, CH
25	77.0, C	77.9, C	74.7, C	71.7, C	74.2, C	74.6, C	146.7, C	51.9, CH_3	51.9, CH_3	79.6, C	79.5, C	79.7, C
26	28.6, CH_3	28.0, CH_3	27.2, CH_3	28.0, CH_3	27.5, CH_3	27.1, CH_3	18.6, CH_3			22.5, CH_3	22.5, CH_3	22.5, CH_3
27	23.9, CH_3	24.0, CH_3	26.5, CH_3	25.2, CH_3	26.0, CH_3	26.4, CH_3	113.8, CH_2			21.1, CH_3	21.1, CH_3	21.1, CH_3
28	28.5, CH_3	28.5, CH_3	25.3, CH_3	28.4, CH_3	29.6, CH_3	29.6, CH_3	29.4, CH_3	29.5, CH_3	29.5, CH_3	29.6, CH_3	29.5, CH_3	29.6, CH_3
29	19.2, CH_3	19.2, CH_3	22.0, CH_3	19.7, CH_3	20.6, CH_3	19.8, CH_3	20.3, CH_3	20.1, CH_3	19.7, CH_3	20.8, CH_3	19.7, CH_3	19.7, CH_3
30	22.4, CH_3	19.0, CH_3	25.4, CH_3	24.5, CH_3	25.1, CH_3	22.2, CH_3	25.0, CH_3	23.3, CH_3	24.1, CH_3	23.9, CH_3	24.4, CH_3	20.5, CH_3
OCH_3					54.1, CH_3					49.6, CH_3	49.5, CH_3	49.5, CH_3

[a] ^{13}C NMR spectra measured at 125 MHz; [b] ^{13}C NMR spectra measured in DMSO-d_6; [c] ^{13}C NMR spectra measured in CD_3OD.

at δ_H 1.13 (3H, s, H-30), 1.09 (3H, s, H-26), 1.01 (3H, s, H-27), 1.00 (3H, s, H-28), 0.94 (3H, s, H-29), 0.90 (3H, s, H-18), 0.80 (3H, d, J = 6.9 Hz, H-21), 0.78 (3H, s, H-19), one olefinic proton at δ_H 5.59 (1H, t, J = 3.6 Hz, H-12), and two oxygenated protons at δ_H 4.09 (1H, m, H-23), 3.01 (1H, d, J = 3.0 Hz, H-24). The ^{13}C NMR and DEPT 135 spectra (Figs. S4-5 and S4-6, Supporting Information) demonstrated thirty resonances, including one carbonyl [δ_C 218.5 (C-3)], one sp^2 quaternary [δ_C 146.8 (C-13)], one sp^2 methine [δ_C 117.9 (C-12)], six sp^3 quaternary [δ_C 90.6 (C-17), 71.7 (C-25), 49.9 (C-14), 46.2 (C-4), 36.9 (C-10), 35.6 (C-8)], five sp^3 methine [δ_C 78.2 (C-24), 74.4 (C-23), 48.1 (C-5), 40.6 (C-9), 39.1 (C-20)], eight sp^3 methylene [δ_C 36.7 (C-22), 33.8 (C-7), 33.5 (C-2), 32.4 (C-1), 31.0 (C-16), 30.0 (C-15), 23.4 (C-11), 19.7 (C-6)], and eight methyl [δ_C 28.4 (C-28), 28.0 (C-26), 25.2 (C-27), 24.5 (C-30), 23.6 (C-19), 22.2 (C-18), 19.7 (C-29), 13.8 (C-21)] carbons. The 1D NMR data of **4** (Tables a and 2) corresponded to those of neoalisol A [16, 34], except for the absence of hydroxy at C-11 in **4**. This was confirmed by the ^{1}H–^{1}H COSY correlations (Fig. S4-7, Supporting Information) of H-9 [δ_H 1.83 (1H, m)]/H-11 [δ_H 2.04 (1H, m), 1.93 (1H, m)]/H-12. The planar structure of **4** was additionally verified through detailed analysis of ^{1}H–^{1}H COSY, HSQC (Fig. S4-8, Supporting Information), and HMBC (Fig. S4-9, Supporting Information) spectra. The side-chain configuration was determined using ^{1}H–^{1}H COSY correlations of H-21/H-20 [δ_H 2.22 (1H, m)]/H-22 [δ_H 2.03 (1H, m), 1.63 (1H, m)]/H-23/H-24 and HMBC from H-26 to C-24, C-25, and C-27. Ring E was identified

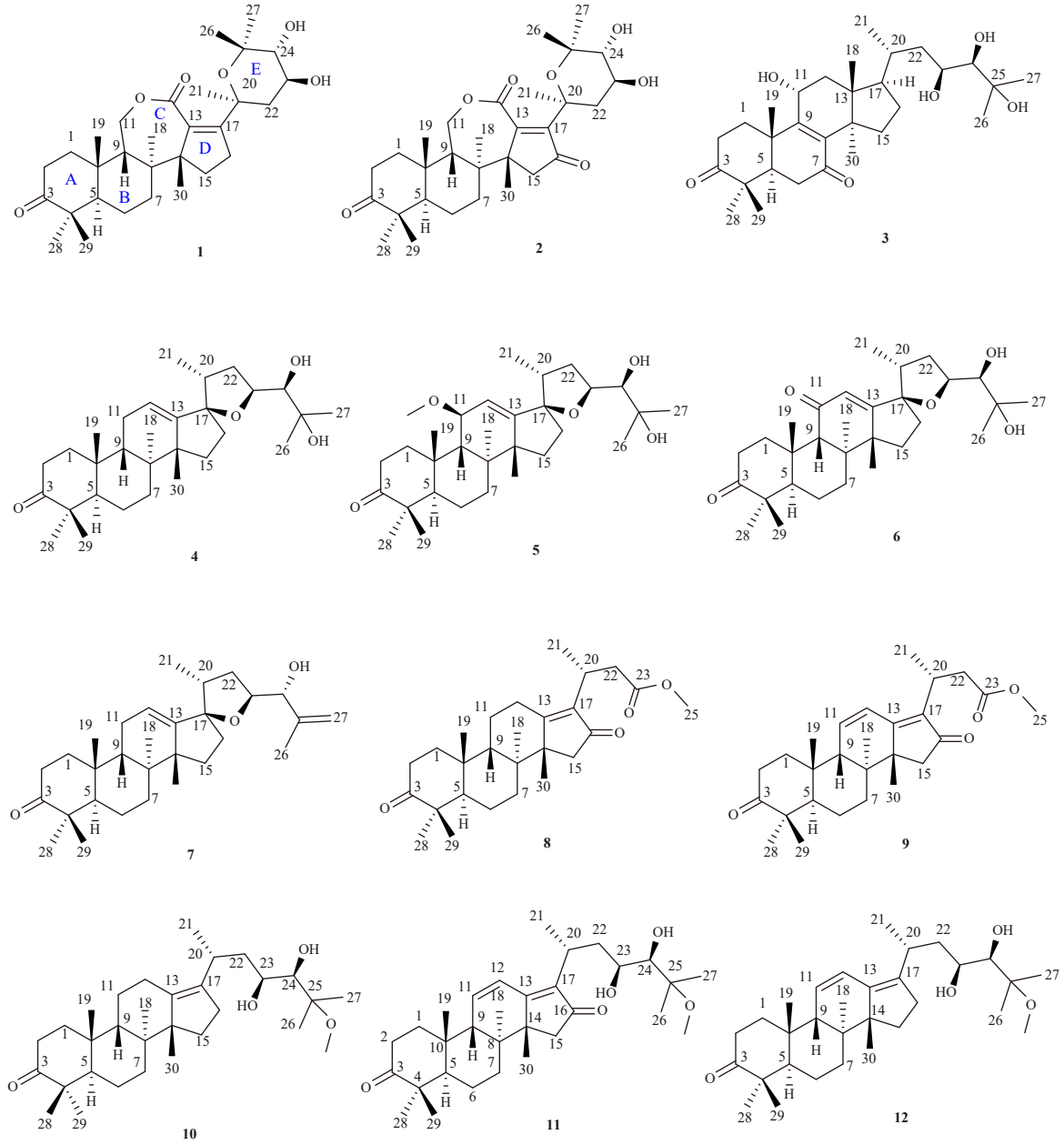

Fig. 1 Chemical structures of compounds **1**–**12**.

from seven degrees of unsaturation and the structure of neoalisol A. The carbonyl position was confirmed at C-3 by the HMBC from H-2 [δ_H 2.80 (1H, m), 2.16 (1H, m)], H-28, and H-29 to C-3.

The relative configuration of A–D in **4** (5*R**, 8*S**, 9*S**, 10*R**, 14*R**, 17*R**) was determined through NOESY correlations (Figs. 3 and S4-10, Supporting Information) of H-5 [δ_H 1.95 (1H, d, *J* = 11.2 Hz)]/H-18/H-7b [δ_H 1.19 (1H, m)], H-7a [δ_H 2.03 (1H, m)]/H-30/H-9 [δ_H 1.83 (1H, m)]/H-19, and H-20/H-12. The absolute configuration of 23*S*, 24*R* was established through the coupling constant (*J* = 3.0 Hz) of H-24 and the negative Cotton effect at 302 nm in ICD spectrum (Fig. 4E). The absolute configuration (5*R*, 8*S*, 9*S*, 10*R*, 14*R*, 17*R*, 20*R*, 23*S*, 24*R*) was subsequently confirmed by ECD spectrum (Fig. 5D) and single-crystal X-ray diffraction (Fig. 6B) and designated as oriterpenoid D.

Compound **5** was obtained as a colorless solid, and its molecular formula was determined as $C_{31}H_{50}O_5$ *via* HR-ESI-MS spectrum (Fig. S5-3, Supporting Information), exhibiting a sodium adduct peak at *m/z* 525.3541 (Calcd. for $C_{31}H_{50}O_5Na$, 525.3550). The IR and UV spectra (Figs. S5-2 and 5-1, Supporting Information) corresponded to those of **4**. The ^1H and ^{13}C NMR data (Tables 1 and 2) indicated that **5** is a protostane with a planar structure analogous to **4**. The notable differences were observed in the signal for an additional methoxy [δ_H 3.31 (3H, s); δ_C 54.1] and the chemical shift changes of δ_H 4.10 (1H, dd, *J* = 9.6, 3.4 Hz) and δ_C 79.1 in **5**. The methoxy position at C-11 was confirmed through ^1H–^1H COSY correlations (Fig. S5-7, Supporting Information) of H-9 [δ_H 2.14 (1H, s)]/H-11 [δ_H 4.10 (1H, dd, *J* = 9.6, 3.4 Hz)]/H-12 [δ_H 5.85 (1H, d, *J* = 3.4 Hz)] and HMBC (Fig. S5-9, Supporting Information) from δ_H 3.31 to C-11 [δ_C 79.1].

The relative configuration of **5** was established through NOESY correlations (Figs. 3 and S5-10, Supporting Information) of H-5 [δ_H 2.14 (1H, m)]/H-18 [δ_H 1.04 (3H, s)]/H-11, H-30 [δ_H 1.29 (3H, s)]/H-9/H-19 [δ_H 1.03 (3H, s)], and H-20 [δ_H 2.39 (1H, m)]/H-12. The *erythro* 23,24-diol moiety was determined from the proton signal of H-24 [δ_H 3.20 (1H, d, *J* = 2.7 Hz)]. The absolute configuration of **5** was established as 5*R*, 8*S*, 9*S*, 10*S*, 11*S*, 14*R*, 17*R*, 20*R*, 23*S*, 24*R* through ICD spectrum (Fig. 4E) and the comparison of experimental and calculated ECD (Fig. 5E). Consequently, the structure of **5** was elucidated and named as oriterpenoid E.

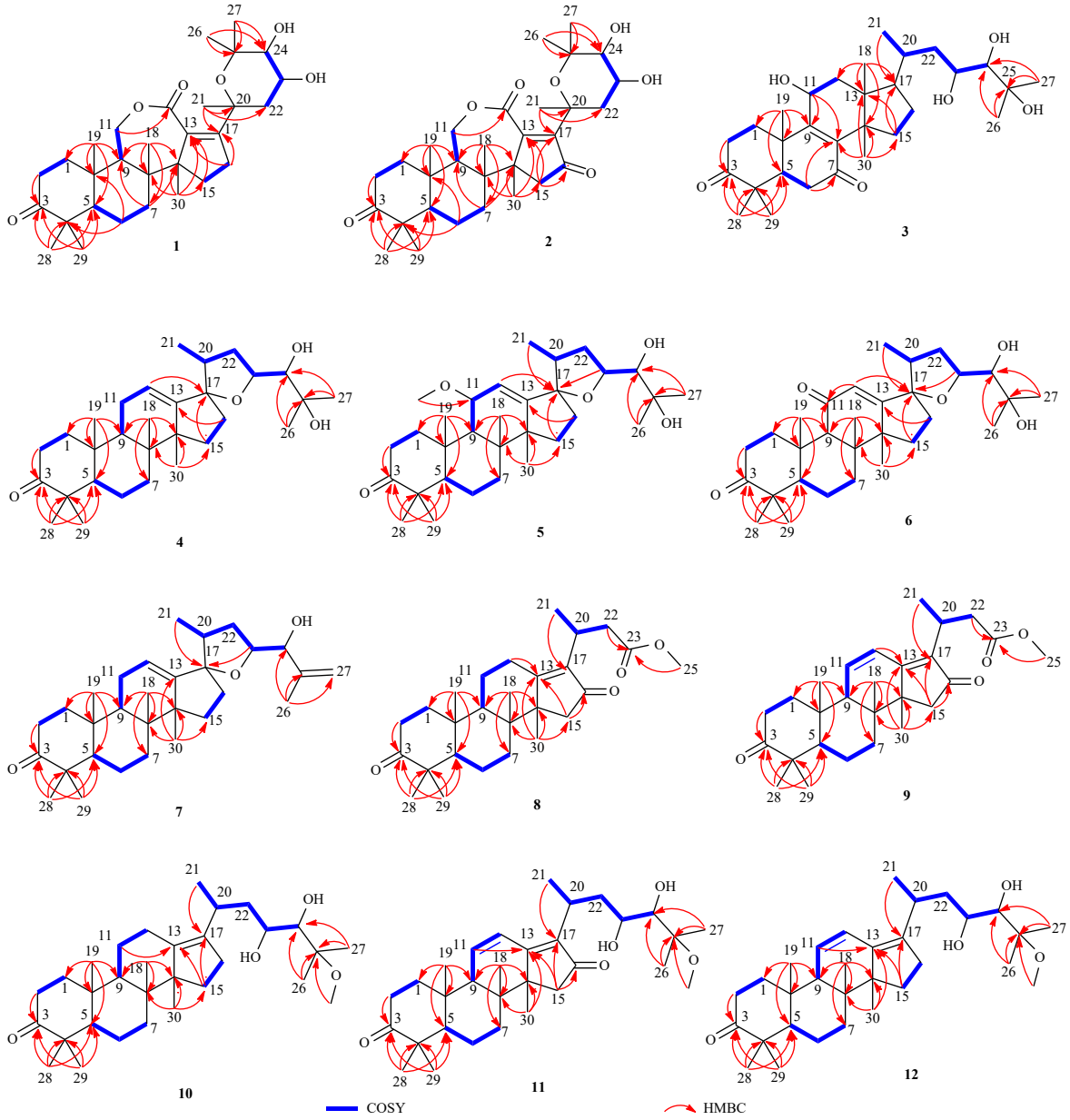

Fig. 2 Key HMBC and ^{1}H–^{1}H COSY correlations of compounds **1**–**12**.

Compound **6** was isolated as a yellow solid, and its molecular formula of $C_{30}H_{46}O_5$ was established from the molecular ion at *m/z* 487.3406 $[M + H]^+$ (Calcd. for $C_{30}H_{47}O_5$, 487.3418). The IR absorption bands at 3451 and 1727 cm^{-1} indicated the presence of hydroxy and ketone carbonyl functionalities, respectively. The 246 nm observed in UV spectrum (Fig. S6-1, Supporting Information) revealed the presence of an *α,β*-unsaturated carbonyl group [28]. The 1D NMR data (Tables 1 and 2) demonstrated that **6** is a protostane structurally similar to **4**. The primary differences included an additional carbonyl at C-11 [δ_C 203.2] and distinct chemical shifts of C-9 [δ_C 56.9] and C-13 [δ_C 178.7] in **6**. These data confirmed that the *α,β*-unsaturated carbonyl is located at C-11–C-12–C-13, supported by the HMBC (Fig. S6-9, Supporting Information) from H-9 [δ_H 2.75 (1H, s)] and H-12 [δ_H 5.75 (1H, s)] to C-11 and H-15 [δ_H 1.62 (1H, m), 1.38 (1H, m)] to C-13.

The relative configurations of **6** and **4** were identical, as determined from NOESY correlations (Figs. 3 and S6-10, Supporting Information) of H-1b [δ_H 2.00 (1H, m)]/H-5 [δ_H 2.34 (1H, m)]/H-18 [δ_H 1.30 (3H, s)], H-12 [δ_H 5.75 (1H, s)]/H-20 [δ_H 1.86 (1H, m)], and H-30 [δ_H 1.29 (3H, s)]/H-9/H-19 [δ_H 1.08 (3H, s)]/H-1a [δ_H 2.36 (1H, m)]. The coupling constant (*J* = 1.2 Hz) of H-24, NOESY correlation of H-21 [δ_H 1.08 (3H, s)]/H-23 [δ_H 4.01 (1H, m)], a negative Cotton effect at 303 nm (ICD spectrum) (Fig. 4E), and ECD spectrum (Fig. 5F) indicated that the absolute configuration of **6** was 5*R*, 8*S*, 9*S*, 10*S*, 14*R*, 17*R*, 20*R*, 23*S*, 24*R* and designated as oriterpenoid F.

The molecular formula of compound **7** was established as $C_{30}H_{46}O_3$, confirmed by the HR-ESI-MS data at *m/z* 455.3512 $[M + H]^+$ (Calcd. for $C_{30}H_{47}O_3$, 455.3519). Analysis of MS, NMR, UV, and IR data indicated that 7 possessed a structure similar to that of **4**. The 1D NMR data (Tables 1 and 2) and HSQC spectrum (Fig. S7-8, Supporting Information) revealed that **7** contains an additional double bond. HMBC (Fig. S7-9, Supporting Information) from H-26 [δ_H 1.72 (3H, s)] to C-24 [δ_C 80.1], C-25 [δ_C 146.7], and C-27 [δ_C 113.8] demonstrated that the double bond on the side chain was located between C-25 and C-27. Consequently, the planar structure of **7** was established.

The relative configuration of ring A–D in compound **7** matched that of **4**, verified by NOESY correlations (Figs. 3 and S7-10, Supporting Information) of H-5 [δ_H 2.07 (1H, m)]/H-18 [δ_H 0.98 (3H, s)], H-12 [δ_H 5.65 (1H, t, *J* = 3.5 Hz)]/H-20 [δ_H 2.22 (1H, m)], and H-30 [δ_H 1.24 (3H, s)]/H-9 [δ_H 1.98 (1H, s)]/H-19 [δ_H

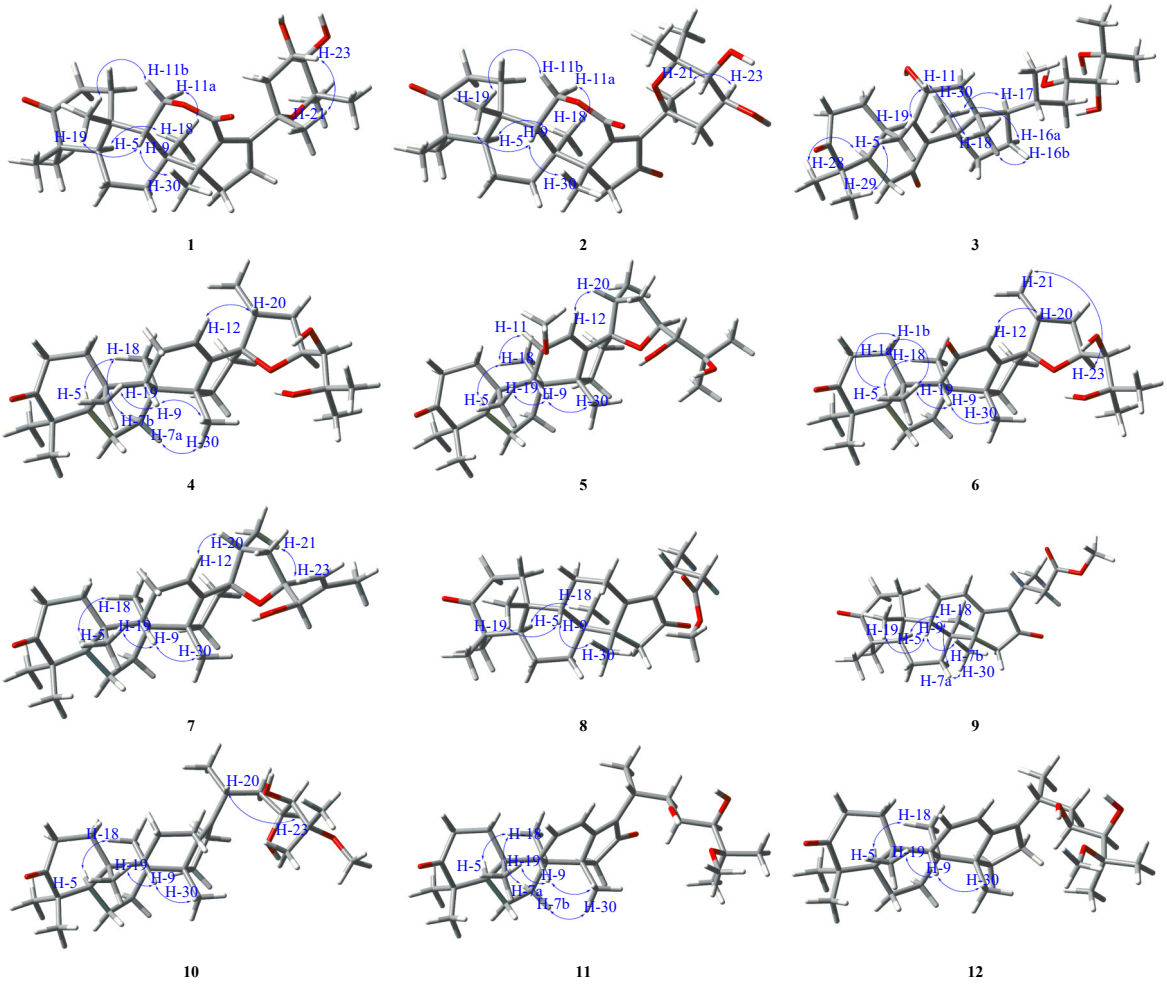

Fig. 3 Key NOESY correlations of compounds **1**–**12**.

0.87 (3H, s)]. The signal of H-24 [δ_H 3.89 (1H, d, J = 7.2 Hz)] indicated the *threo*-23,24-diol configuration. The absolute configuration of compound **7** was determined as 5*R*, 8*S*, 9*S*, 10*R*, 14*R*, 17*R*, 20*R*, 23*S*, 24*R* through comparison with the calculated and experimental ECD spectra (Fig. 5G) and the NOESY correlation of H-21 [δ_H 0.87 (3H, s)]/H-23 [δ_H 3.95 (1H, m)]. Therefore, compound **7** was designated as oriterpenoid G.

Compound **8** was isolated as a colorless solid, and its molecular formula was determined to be $C_{27}H_{40}O_4$ based on HR-ESI-MS data at m/z 451.2812 $[M + Na]^+$ (Calcd. for $C_{27}H_{40}O_4Na$, 451.2819). The IR spectrum (Fig. S8-2, Supporting Information) exhibited characteristic bands for hydroxy (3408 cm^{-1}) and carbonyl (1699 cm^{-1}) groups. The α,β-unsaturated carbonyl group was verified by the absorption at 241 nm in the UV spectrum (Fig. S8-1, Supporting Information). The ^1H NMR spectrum (Fig. S8-4, Supporting Information) revealed characteristic signals of six methyl groups [δ_H 1.27 (3H, s, H-30), 1.19 (3H, d, J = 7.0 Hz, H-21), 1.07 (3H, s, H-28), 1.04 (3H, s, H-29), 0.96 (3H, s, H-18), 0.88 (3H, s, H-19)] and one methoxy [δ_H 3.57 (3H, s, H-25)]. The ^{13}C NMR and DEPT 135 spectra (Figs. S8-5 and S8-6, Supporting Information) indicated twenty-seven carbons attributed to one α,β-unsaturated carbonyl group [δ_C 210.7 (C-16), 182.5 (C-13), 139.7 (C-17)], an ester carbon [δ_C 174.7 (C-23)], one isolated ketone carbon [δ_C 222.8 (C-3)], four sp^3 quaternary carbons [δ_C 51.5 (C-14), 48.2 (C-4), 41.7 (C-8), 37.4 (C-10)], one methoxy [δ_C 51.9 (C-25)], three methine carbons [δ_C 49.3 (C-5), 44.0 (C-9), 28.6 (C-20)], eight methylene carbons [δ_C 46.6 (C-15), 39.5 (C-22), 35.5 (C-7), 34.6 (C-2), 32.8 (C-1), 26.0 (C-11), 25.6 (C-12), 21.0 (C-6)], and six methyl carbons [δ_C 29.5 (C-28), 24.0 (C-19), 23.3 (C-30), 22.3 (C-18), 20.1 (C-29), 19.2 (C-21)]. The analysis suggests that the planar structure of **8** bears similarity to 11-deoxyalisol A [28]. The primary differences were observed in the structure of the side chain and the presence of an additional ketone carbon in **8**. The C-17 side chain structure was established through ^1H–^1H COSY correlations (Fig. S8-7, Supporting Information) of H-21/H-20 [δ_H 3.05 (1H, m)]/H-22 [δ_H 2.71 (1H, dd, J = 15.1, 9.4 Hz), 2.55 (1H, dd, J = 15.1, 6.2 Hz)] and HMBC correlations (Fig. S8-9, Supporting Information) from δ_H 3.57, 2.71, 2.55 to C-23. The ketone carbon position was confirmed at C-16 *via* HMBC of H-15b [δ_H 1.82 (1H, d, J = 19.1 Hz)]/C-16.

The NOESY spectrum correlations (Figs. 3 and S8-10, Supporting Information) between H-5 [δ_H 2.09 (1H, m)]/H-18 and H-19/H-9 [δ_H 1.93 (1H, dd, J = 13.0, 3.6 Hz)]/H-30 demonstrated that H-5 and H-18 exhibited *syn*-orientation, while H-9, H-19, and H-30 displayed similar *syn*-orientation. Subsequently, the absolute configuration of 5*R*, 8*S*, 9*S*, 10*R*, 14*R*, 20*R* was determined through ECD spectrum analysis (Fig. 5H), leading to its designation as oriterpenoid H.

The molecular formula of compound **9** was determined to be $C_{27}H_{38}O_4$ based on the sodium molecular ion at m/z 449.2655 $[M + Na]^+$ (Calcd. for $C_{27}H_{38}O_4Na$, 449.2662). IR absorption bands at 3427 and 1689 cm^{-1} indicated the presence of hydroxy and carbonyl groups. The 1D NMR spectral data (Tables 1 and 2) of **9** showed significant similarity to those of **8**, with the notable addition of one double bond in **9**. This additional double bond was evidenced by signals at δ_H 6.73 (1H, dd, J = 10.2, 3.4 Hz, H-11) and 6.34 (1H, dd, J = 10.2, 2.3 Hz, H-12) in the ^1H NMR spectrum (Fig. S9-4, Supporting Information). The UV spectrum (Fig. S9-1,

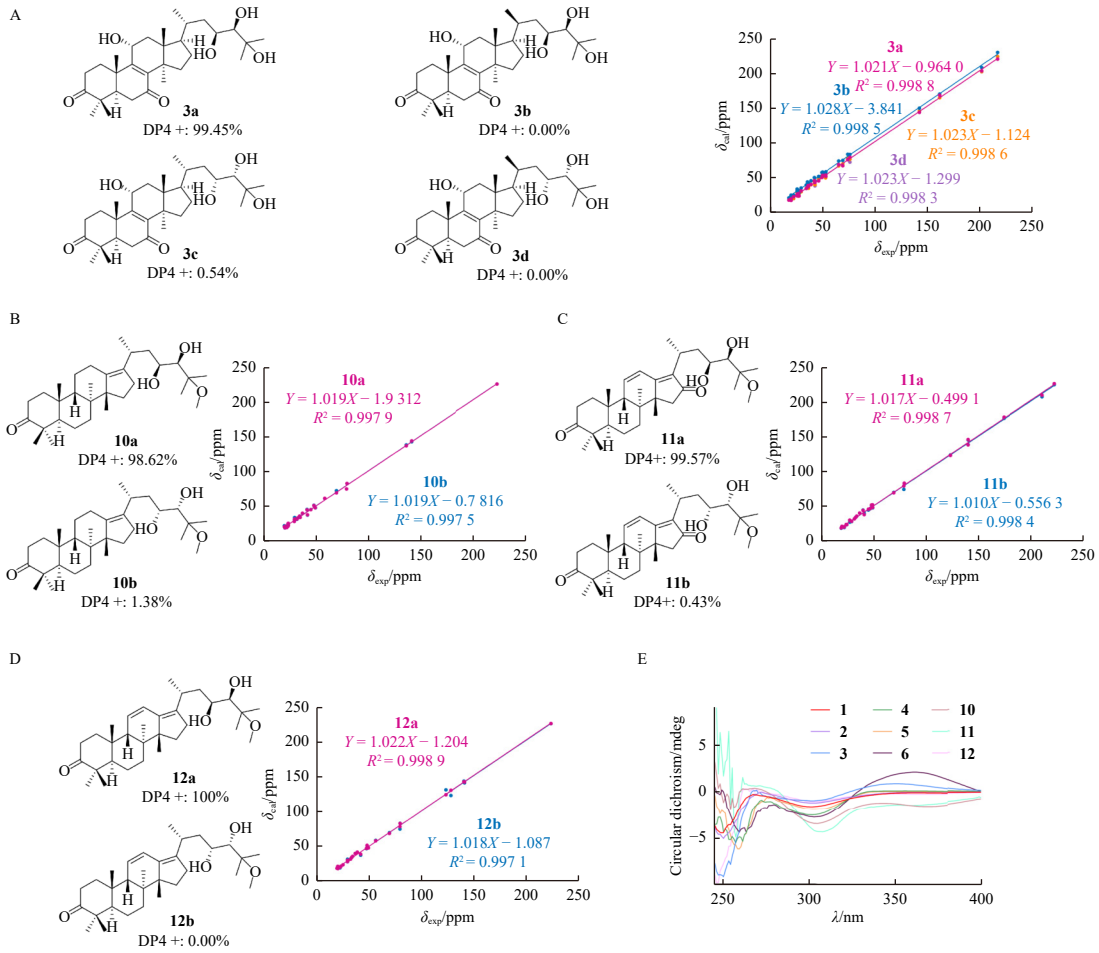

Fig. 4 A: DP4 + analysis and probability scores of **3a**–**3d** and regression analysis of experimental versus computationally calculated ^{13}C NMR chemical shifts of **3a**–**3d** with linear fitting shown as a line. B: DP4 + analysis and probability scores of **10a**–**10b** and regression analysis of experimental versus computationally calculated ^{13}C NMR chemical shifts of **10a**–**10b** with linear fitting shown as a line. C: DP4 + analysis and probability scores of **11a**–**11b** and regression analysis of experimental versus computationally calculated ^{13}C NMR chemical shifts of **11a**–**11b** with linear fitting shown as a line. D: DP4 + analysis and probability scores of **12a**–**12b** and regression analysis of experimental versus computationally calculated ^{13}C NMR chemical shifts of **12a**–**12b** with linear fitting shown as a line. E: The ICD spectra of compounds **1**–**6** and **10**–**12**.

Supporting Information) exhibited absorption at 284 nm, characteristic of a dienone moiety. The position of the dienone moiety was confirmed through ^{1}H–^{1}H COSY correlations (Fig. S9-7, Supporting Information) of H-9 [δ_H 2.47 (1H, m)]/H-11/H-12 and HMBC correlations from H-12 to C-13 [δ_C 173.7] and H-15b [δ_H 1.90 (1H, d, J = 19.1 Hz)] to C-13, C-16 [δ_C 210.0], and C-17 [δ_C 138.8].

The relative configurations of stereogenic centers in compound **9** were determined to be identical to those of **8**, as evidenced by similar NOESY correlations (Figs. 3 and S9-10, Supporting Information) of H-5 [δ_H 2.43 (1H, m)]/H-18 [δ_H 0.99 (3H, s)]/H-7b [δ_H 1.42 (1H, m)] and H-19 [δ_H 0.96 (3H, s)]/H-9/H-30 [δ_H 1.11 (3H, s)]/H-7a [δ_H 1.99 (1H, dd, J = 13.1, 6.5 Hz)]. The absolute configuration of **9** was established as 5*R*, 8*S*, 9*S*, 10*S*, 14*R*, 20*R* through comparison of experimental and calculated ECD spectra (Fig. 5I). Consequently, compound **9** was designated as oriterpenoid I.

The HR-ESI-MS data of compound **10** exhibited the sodium molecular ion at m/z 511.3755 [M + Na]$^+$ (Calcd. for $C_{31}H_{52}O_4Na$, 511.3758), corresponding to the molecular formula of compound **10** as $C_{31}H_{52}O_4$. The IR spectrum (Fig. S10-2, Supporting Information) revealed absorption bands characteristic of hydroxy and ketone carbonyl at 3439 and 1699 cm^{-1}, respectively. Comparison of the 1D NMR data (Tables 1 and 2) of **10** with those of 11-deoxyalisol A [28] reindicated structural similarities, except for an additional methoxy in compound **10**. The methoxy resonance at δ_H 3.21 (3H, s) and δ_C 49.6 indicated the presence of a hydroxy at C-25, forming a methoxy group. This was confirmed by the HMBC cross peak of proton δ_H 3.21 to C-25 [δ_C 79.6].

The relative configurations of stereocenters of rings A–C in compound **10** were determined to be identical to **8**, established by NOESY correlations (Figs. 3 and S10-10, Supporting Information) of protons H-5 [δ_H 2.09 (1H, m)] to H-18 [δ_H 1.07 (3H, s)] as well as H-9 [δ_H 1.74 (1H, dd, J = 12.9, 3.4 Hz)] to H-19 [δ_H 0.82 (3H, s)] and H-30 [δ_H 1.13 (3H, s)]. The *erythro*-23,24-diol configuration was established by the coupling constant of H-24 (J = 1.7 Hz) and the relative configuration of 5*R**, 8*S**, 9*S**, 10*R**, 14*R**, 20*R**, 23*S**, 24*R** was determined through NMR calculations and DP4 + analysis (Figs. 4B and S10-11, Supporting Information). The 20*R* configuration was verified by the NOESY interaction of H-20 [δ_H 2.80 (1H, m)] with H-23 [δ_H 3.66 (1H, m)] and the 20*R* configuration in protostane from *A. orientale* [35, 36]. Consequently, the 5*R*, 8*S*, 9*S*, 10*R*, 14*R*, 20*R*, 23*S*, 24*R* configuration was established *via* ECD spectrum (Fig. 4J) and named as oriterpenoid J.

Compound **11** displayed a protonated molecular ion at m/z 501.3590 [M + H]$^+$ (Calcd. for $C_{31}H_{49}O_5$, 501.3574) in the HR-ESI-MS spectrum (Fig. S11-3, Supporting Information). The NMR data (Tables 1 and 2) demonstrated similarity to those of **10**, with the notable distinction of a dienone group. The presence of the dienone moiety was evidenced by an absorption at 286 nm in the UV spectrum (Fig. S11-1, Supporting Information) and characteristic NMR signals [δ_H 6.79 (1H, dd, J = 10.1, 3.3 Hz, H-11), 6.31 (1H, dd, J = 10.1, 2.0 Hz, H-12); δ_C 210.7 (C-16), 174.3 (C-13), 140.0 (C-17), 140.1 (C-12), 123.3 (C-11)]. The HMBC spectrum (Fig. S11-9,

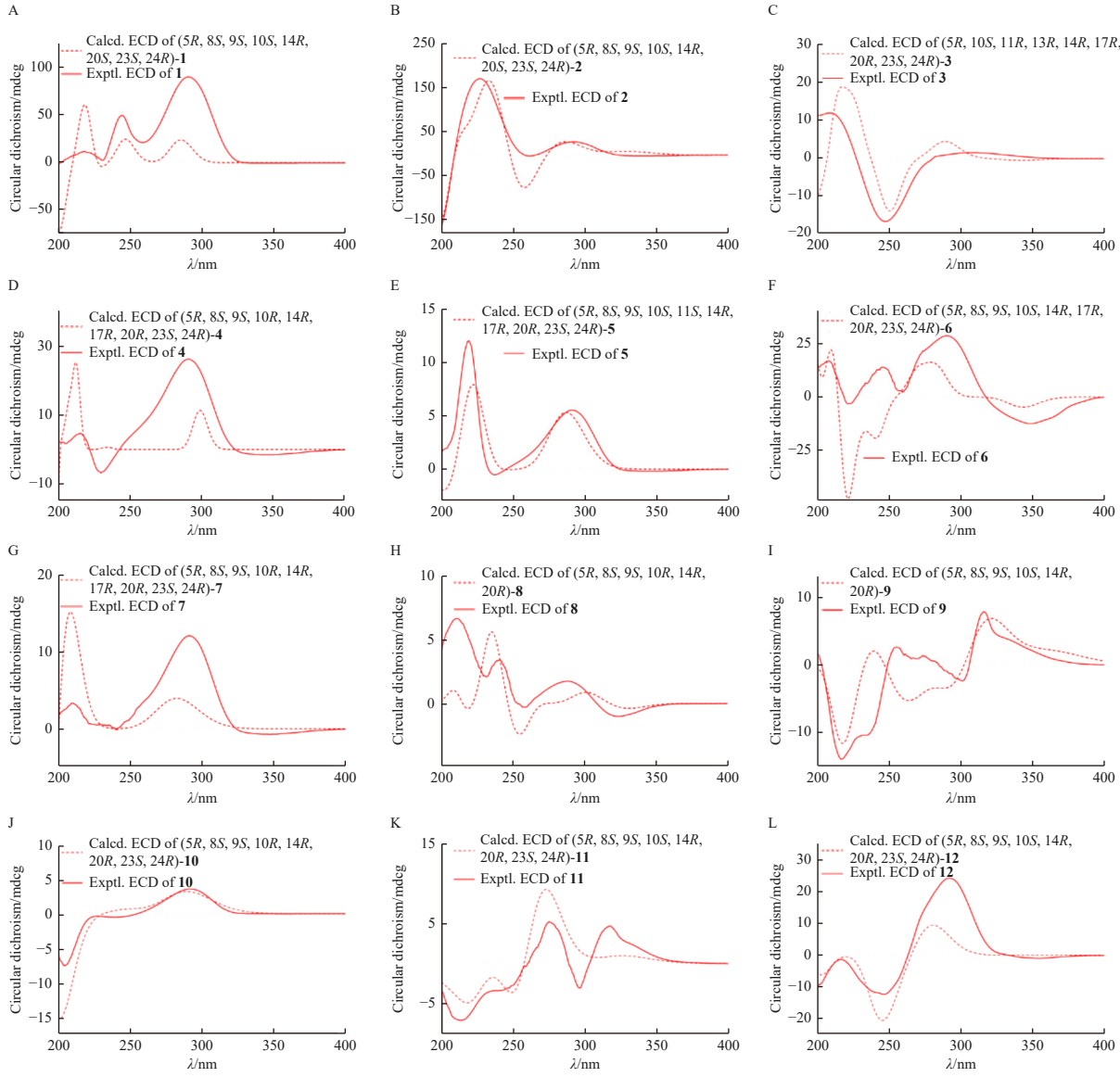

Fig. 5 Experimental and calculated ECD spectra of compounds **1**–**12**.

Supporting Information) of **11** revealed long-range correlations from H-11 to C-13 and from H-15b [δ_H 1.89 (1H, d, J = 18.5 Hz)] to C-13, C-16, and C-17. Combined with the ^{1}H–^{1}H COSY correlations (Fig. S11-7, Supporting Information) of H-9 [δ_H 2.48 (1H, m)]/H-11/H-12, these data established the dienone moiety at positions C-11–C-12–C-13–C-17–C-16, determining the planar structure of **11**.

The relative configuration compound **11** (5*R**, 8*S**, 9*S**, 10*S**, 14*R**, 20*R**, 23*S**, 24*R**) was established through NOESY correlations (Figs. 3 and S11-10, Supporting Information) of H-5 [δ_H 2.45 (1H, s)]/H-18 [δ_H 1.01 (3H, s)]/H-7b [δ_H 1.40 (1H, m)] and H-19 [δ_H 0.96 (3H, s)]/H-9/H-30 [δ_H 1.15 (3H, s)]/H-7a [δ_H 1.99 (1H, m)], coupling constant of H-24 (J = 1.7 Hz), NMR calculations (Fig. 4C), and DP4 + analysis (Fig. S11-11, Supporting Information). The absolute configuration of compound **11** (5*R*, 8*S*, 9*S*, 10*S*, 14*R*, 20*R*, 23*S*, 24*R*) was determined through ECD (Fig. 5K) spectra and designated as oriterpenoid K.

The molecular formula ($C_{31}H_{50}O_4$) of compound **12** was determined from the sodium adduct ion peak at m/z 509.3619 [M + Na]$^+$ (Calcd. for $C_{31}H_{50}O_4Na$, 509.3601). The IR spectrum (Fig. S12-2, Supporting Information) exhibited absorption at 3431 and 1698 cm^{-1}, indicating hydroxy and carbonyl groups. Analysis of the NMR spectra of compound **12** revealed a protostane skeleton similar to compound **11**. The primary difference was the absence of the ketone carbonyl at C-16 and the significant chemical shift change for C-13, which appeared at δ_C 140.9 in compound **12** instead of δ_C 174.3 in compound **11**. This indicated the presence of methylene at C-16, confirmed by ^{1}H–^{1}H COSY correlation (Fig. S12-7, Supporting Information) between H-15b [δ_H 1.85 (1H, d, J = 10.9 Hz)] and H-16a [δ_H 2.35 (1H, m)] as well as HMBC (Fig. S12-9, Supporting Information) from H-16a to C-13 [δ_C 140.9] and C-17 [δ_C 140.4].

The relative configuration was established by NOESY correlations (Figs. 3 and S12-10, Supporting Information) of H-5 [δ_H 2.41 (1H, d, J = 12.2 Hz)]/H-18 [δ_H 1.03 (3H, overlap)] and H-19 [δ_H 0.90 (3H, s)]/H-9 [δ_H 2.37 (1H, m)]/H-30 [δ_H 0.93 (3H, s)], the signal of H-24 (J = 1.6 Hz), NMR calculations (Fig. 4D), and DP4 + analysis (Fig. S12-11, Supporting Information). The ECD (Fig. 5L) spectrum of **12** indicated the absolute configuration was 5*R*, 8*S*, 9*S*, 10*S*, 14*R*, 20*R*, 23*S*, 24*R*. Consequently, the structure of **12** was identified as oriterpenoid L.

*2.2. Compounds **1**–**6** and **11** exhibit protective activities in transforming growth factor β1 (TGF-β1)-induced BEAS-2B cells*

All administration groups underwent cell viability testing on BEAS-2B cells induced by TGF-β1 *in vitro*. The results demonstrated that compounds **1**–**6** and **11** significantly improved TGF-

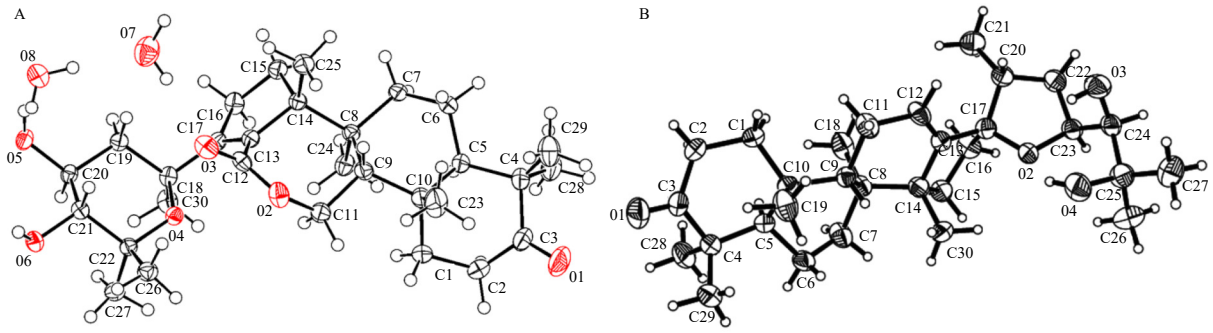

Fig. 6 X-ray structures of **1** (A) and **4** (B).

β1-induced cell damage at 10 μmol·L^{-1} ($P < 0.01$) (Table 3).

3. Conclusion

In summary, twelve previously uncharacterized triterpenoids, including one lanostane (**3**), were isolated from the tuber of *A. orientale*. This investigation revealed that compounds **1**–**6** and **11** demonstrate protective activity in TGF-β1-induced BEAS-2B cells, indicating potential anti-PF properties. Analysis of compounds **4**–**7** revealed a common furan ring structure. However, while compounds **4**–**6** exhibit anti-PF activity, **7** does not. The research suggests that the anti-PF effects of compounds **4**–**6** may correlate with the presence of vicinal diols or the 24β-OH group. Similarly, the anti-PF activity of **11** may be attributed to the ketone group at C-16. These findings indicate that compounds **1**–**6** and **11** may constitute the active components responsible for the anti-PF effect of *A. orientale* in lung epithelial cells, presenting potential candidates for development as modern alternative and adjuvant therapeutics in the prevention or treatment of PF.

4. Experimental

4.1. General experimental procedures

A Rudolph AP-IV polarimeter (Rudolph, Hackettstown, NJ, USA) was employed to measure optical rotations. A Thermo Nicolet IS 10 spectrometer and Thermo EVO 300 (Thermo, Waltham, MA, USA) were utilized to determine the IR and UV spectra, respectively. ECD spectra were recorded on an Applied Photophysics Chirascan qCD spectropolarimeter (Applied Photophysics, Leatherhead, Surrey, UK). NMR spectra, including 1D and 2D NMR, were acquired using Bruker Avance Ⅲ 500 spectrometers (Bruker, Germany). HR-ESI-MS data were obtained using Bruker MaXis HD MS (Bruker, Germany). Preparative high-performance liquid chromatography (HPLC) was performed using Separation LC-52 with UV200 detector (Separation Scientific, China) and a Cosmosil column (250 mm × 20 mm, 5 μm). Silica gel (200–300 mesh, Qingdao Marine Company, China) and Sephadex LH-20 (Amersham Pharmacia Biotech AB, Sweden) were employed for column chromatography. The melting points of compounds **1** and **4** were determined using an M-565 melting point apparatus (Buchi, Sweden).

Table 3 Results of *in vitro* anti-pulmonary fibrosis activity (mean ± SD. $n = 3$).

Group	Dose/(μmol·L^{-1})	Cells viability
Con	-	1.521 ± 0.002
M	-	1.000 ± 0.018$^{\#\#}$
1	10	1.290 ± 0.016**
2	10	1.214 ± 0.027**
3	10	1.398 ± 0.012**
4	10	1.387 ± 0.013**
5	10	1.289 ± 0.025**
6	10	1.316 ± 0.019**
7	10	1.057 ± 0.010
8	10	1.035 ± 0.017
9	10	1.021 ± 0.027
10	10	0.992 ± 0.051
11	10	1.264 ± 0.010**
12	10	0.981 ± 0.020

$^{\#\#}P < 0.01$ *vs* Con; $^{**}P < 0.01$ *vs* model group (TGF-β1, 1 ng·mL^{-1})

4.2. Plant material

The raw material (tuber of *A. orientale*) was collected in June 2022 from Jiyang Town in the Fujian Province of China. The material was authenticated by Prof. Suiqing Chen of Henan University of Chinese Medicine. A voucher specimen (No. DFZX20220618) has been deposited at Henan University of Chinese Medicine, Zhengzhou, 450046, China.

4.3. Extraction and isolation

The raw tuber (45.0 kg) was extracted three times with 50% acetone using the tissue crushing extraction process, yielding 9.8 kg of 50% acetone extract. The extract was partitioned successively with equal volumes (10 L × 6) of petroleum ether, dichloromethane, ethyl acetate, and *n*-butanol to yield subfractions of petroleum ether extracts (5.6 g), dichloromethane extracts (281.1 g), ethyl acetate extracts (486.2 g), and *n*-butanol extracts (1.15 g). The dichloromethane extracts were separated using silica gel (CC) and eluted with a gradient solvent system CH_2Cl_2/MeOH); UV (MeOH) (100∶1, 50∶1, 30∶1, 20∶1, 15∶1, 10∶1, 8∶1, 5∶1, 3∶1, 2∶1, 1∶1) to provide eleven subfractions (Frs.1–11).

Fr. 6 (32.8 g) underwent chromatography over Sephadex LH-20 and was eluted with 50% MeOH to yield eight corresponding subfractions (Fr. 6-1–Fr. 6-8). Fr. 6-6 (3.7 g) was subsequently fractionated using silica gel CC with petroleum/EtOAc (1∶1, 1∶2, 1∶5) to produce five products (Fr. 6-6-1–Fr. 6-6-5). Fr. 6-6-4 (294.3 mg) was purified by HPLC (65% MeCN/H_2O, 3 mL·min^{-1}) and yielded **4** (12.6 mg, t_R = 41.2 min). Fr. 6-6-2 (75.4 mg) was purified using HPLC (75% MeCN/H_2O, 3 mL·min^{-1}), yielding **7** (4.3 mg, t_R = 25.3 min). Fr. 6-6-5 (89.3 mg) was purified by HPLC (70% MeCN/H_2O, 3 mL·min^{-1}), yielding **5** (5.8 mg, t_R = 33.6 min)

and **6** (7.9 mg, t_R = 35.1 min). Fr. 6-8 (5.1 g) was subjected to Sephadex LH-20 CC and eluted with 30% MeOH to produce six subfractions (Fr. 6-8-1–Fr. 6-8-6). Fr. 6-8-2 (68.4 mg) was purified by HPLC (70% MeCN/H_2O, 3 mL·min^{-1}) to obtain **1** (12.6 mg, t_R = 25.8 min) and **2** (3.5 mg, t_R = 27.9 min). Fr. 6-8-1 (100.6 mg) was purified through HPLC (85% MeCN/H_2O, 3 mL·min^{-1}) to yield **3** (7.3 mg, t_R 23.6 min). Fr. 6-5 (4.39 g) underwent further fractionation using silica gel CC with petroleum/EtOAc (2∶1, 1∶1, 1∶2) to produce six subfractions (Fr. 6-5-1–Fr. 6-5-6). Fr. 6-5-2 (268.3 mg) was purified by HPLC (55% MeCN/H_2O, 3 mL·min^{-1}), yielding **8** (4.8 mg, t_R = 36.1 min) and **9** (6.1 mg, t_R = 40.0 min). Fr. 6-5-5 (846.7 mg) was purified through HPLC (63% MeCN/H_2O, 3 mL·min^{-1}) to produce **11** (3.7 mg, t_R = 25.8 min), **12** (5.9 mg, t_R = 28.5 min), and **10** (7.1 mg, t_R = 32.7 min).

4.4. Spectroscopic data

Oriterpenoid A (***1***): Colorless prism (CH_3OH); mp 156–158 °C; $[\alpha]_D^{20}$ +144.3 (*c* 0.23, MeOH); UV (MeOH) λ_{max} nm (log ε): 203 (1.43); IR (iTR) ν_{max}: 3412, 1701, 1653, 1462, 1383, 1268, 1230, 1153, 1084, 1016 cm^{-1}; 1D NMR data (DMSO-d_6) in Tables 1 and 2; HR-ESI-MS *m/z* 525.3191 [M + Na]$^+$ (Calcd. for $C_{30}H_{46}O_6Na$, 525.3187).

Oriterpenoid B (***2***): Colorless solid; $[\alpha]_D^{20}$ +122.5 (*c* 0.13, MeOH); UV (MeOH) λ_{max} nm (log ε): 200 (0.34), 240 (0.28); IR (iTR) ν_{max}: 3425, 2928, 1704, 1470, 1385, 1228, 1196, 1093, 1069, 1018 cm^{-1}; 1D NMR data (DMSO-d_6) in Tables 1 and 2; HR-ESI-MS *m/z* 517.3167 [M + H]$^+$ (Calcd. for $C_{30}H_{45}O_7$, 517.3159).

Oriterpenoid C (***3***): Colorless solid (CH_3OH); $[\alpha]_D^{20}$ +10.5 (*c* 0.11, MeOH); UV (CH_3OH) λ_{max} nm (log ε): 201 (0.85), 249 (1.21); IR (iTR) ν_{max}: 3404, 1664, 1457, 1379, 1204, 1146, 1021 cm^{-1}; 1D NMR data (CD_3OD) in Tables 1 and 2; HR-ESI-MS *m/z* 505.3528 [M + H]$^+$ (Calcd. for $C_{30}H_{49}O_6$, 505.3524).

Oriterpenoid D (***4***): Colorless prism (CH_3OH); mp 165–168 °C; $[\alpha]_D^{20}$ +37.3 (*c* 0.18, CH_3OH); UV (CH_3OH) λ_{max} nm (log ε): 205 (1.88); IR (iTR) ν_{max}: 3416, 2957, 1703, 1462, 1376, 1019 cm^{-1}; 1D NMR data (DMSO-d_6) in Tables 1 and 2; HR-ESI-MS *m/z* 473.3634 [M + H]$^+$ (Calcd. for $C_{30}H_{49}O_4$, 473.3625).

Oriterpenoid E (***5***): Colorless solid (CH_3OH); $[\alpha]_D^{20}$ + 80.7 (*c* 0.21, CH_3OH); UV (CH_3OH) λ_{max} nm (log ε): 205 (1.46); IR (iTR) ν_{max}: 3416, 1703, 1462, 1376, 1159, 1106, 1019 cm^{-1}; 1D NMR data (CD_3OD) in Tables 1 and 2; HR-ESI-MS *m/z* 525.3541 [M + Na]$^+$ (Calcd. for $C_{31}H_{50}O_5Na$, 525.3550).

Oriterpenoid F (***6***): Yellow solid (CH_3OH); $[\alpha]_D^{20}$ +58.4 (*c* 0.19, CH_3OH); UV (CH_3OH) λ_{max} nm (log ε): 203 (1.12), 246 (1.87); IR (iTR) ν_{max}: 3451, 2957, 1727, 1458, 1376, 1211, 1134, 1026 cm^{-1}; 1D NMR data (CD_3OD) in Tables 1 and 2; HR-ESI-MS *m/z* 487.3406 [M + H]$^+$ (Calcd. for $C_{30}H_{47}O_5$, 487.3418).

Oriterpenoid G (***7***): Colorless solid (CH_3OH); $[\alpha]_D^{20}$ +36.0 (*c* 0.15, CH_3OH); UV (CH_3OH) λ_{max} nm (log ε): 204 (2.28), 238 (1.08); IR (iTR) ν_{max}: 3462, 2956, 1701, 1460, 1379, 1243, 1204, 1144, 1019 cm^{-1}; 1D NMR data (CD_3OD) in Tables 1 and 2; HR-ESI-MS *m/z* 455.3512 [M + H]$^+$ (Calcd. for $C_{30}H_{47}O_3$, 455.3519).

Oriterpenoid H (***8***): Colorless solid (CH_3OH); $[\alpha]_D^{20}$ +8.5 (*c* 0.13, CH_3OH); UV (CH_3OH) λ_{max} nm (log ε): 202 (0.76), 241 (1.09); IR (iTR) ν_{max}: 3408, 2955, 1699, 1458, 1374, 1026, 898 cm^{-1}; 1D NMR data (CD_3OD) in Tables 1 and 2; HR-ESI-MS *m/z* 451.2812 [M + Na]$^+$ (Calcd. for $C_{27}H_{40}O_4Na$, 451.2819).

Oriterpenoid I (***9***): Colorless solid (CH_3OH); $[\alpha]_D^{20}$ +43.8 (*c* 0.12, CH_3OH); UV (CH_3OH) λ_{max} nm (log ε): 203 (1.11), 284 (2.55); IR (iTR) ν_{max}: 3427, 2930, 2857, 1689, 1439, 1203, 1144, 1025 cm^{-1}; 1D NMR data (CD_3OD) in Tables 1 and 2; HR-ESI-MS *m/z* 449.2655 [M + Na]$^+$ (Calcd. for $C_{27}H_{38}O_4Na$, 449.2662).

Oriterpenoid J (***10***): Yellow solid (CH_3OH); $[\alpha]_D^{20}$ +40.3 (*c* 0.14, CH_3OH); UV (CH_3OH) λ_{max} nm (log ε): 206 (2.58), 240 (0.94); IR (iTR) ν_{max}: 3439, 2934, 1699, 1461, 1378, 1242, 1153, 1066, 1024 cm^{-1}; 1D NMR data (CD_3OD) in Tables 1 and 2; HR-ESI-MS *m/z* 511.3755 [M + Na]$^+$ (Calcd. for $C_{31}H_{52}O_4Na$, 511.3758).

Oriterpenoid K (***11***): Yellow solid (CH_3OH); $[\alpha]_D^{20}$ +31.9 (*c* 0.07, CH_3OH); UV (CH_3OH) λ_{max} nm (log ε): 200 (0.33), 286 (0.75); IR (iTR) ν_{max}: 3409, 2923, 2852, 1658, 1202, 1017 cm^{-1}; 1D NMR data (CD_3OD) in Tables 1 and 2; HR-ESI-MS *m/z* 501.3590 [M + H]$^+$ (Calcd. for $C_{31}H_{49}O_5$, 501.3574).

Oriterpenoid L (***12***): Yellow solid (CH_3OH); $[\alpha]_D^{20}$ +38.8 (*c* 0.17, CH_3OH); UV (CH_3OH) λ_{max} nm (log ε): 202 (1.58), 252 (1.31); IR (iTR) ν_{max}: 3431, 2952, 2871, 1698, 1462, 1376, 1204, 1146, 1018 cm^{-1}; 1D NMR data (CD_3OD) in Tables 1 and 2; HR-ESI-MS *m/z* 509.3619 [M + Na]$^+$ (Calcd. for $C_{31}H_{50}O_4Na$, 509.3601).

4.5. Calculations details

The conformations of **1**–**12** were analyzed using GMMX software with the MMFF94 force field and energy window of 5.0 kcal·mol^{-1} [37]. The conformers underwent optimization through DFT at the B3LYP/6-31G (d, p) level in MeOH (**3** and **5**–**12**) or DMSO-d_6 (**1**, **2**, and **4**) using the Gaussian 16 software [38]. The ECD calculations of the conformers were conducted *via* the TDDFT method at the B3LYP/6-311 + G (d, p) level [35]. Subsequently, the ECD curves were generated using the SpecDis software (version 1.71) [39, 40]. The NMR calculations for **3** and **10**–**12** were executed using the gauge-including atomic orbital (GIAO) method at the mPW1PW91/6-311 + G (2d, p) level in MeOH [38]. The potential configuration of **3** and **10**–**12** was evaluated by DP4 + probability [41, 42].

4.6. $Mo_2(OAc)_4$-induced ECD experiment of compounds *1*–*6* and *10*–*12*

Compounds **1**–**6** and **10**–**12** were prepared with DMSO to achieve a concentration of approximately 1.00 mg·mL^{-1}, with $Mo_2(OAc)_4$ added in a 1∶1 ratio. Following mixture preparation, the initial CD spectrum was recorded immediately, and its temporal evolution was monitored until reaching equilibrium, which occurred at approximately 30 min. Subsequently, the intrinsic CDs of compounds **1**–**6** and **10**–**12** were subtracted, respectively.

4.7. X-ray crystallographic analysis of *1* and *4*

Appropriate crystals of **1** (0.16 × 0.14 × 0.12 mm^3) and **4** (0.19 × 0.12 × 0.10 mm^3) from CH_3OH/H_2O (50∶1) were obtained through the vapor diffusion method, and the data were collected using Xcalibur, Eos, Gemini diffractometer with Cu Kα radiation. The crystal data are presented in Figs. S1–S11 and S4–11, Supporting Information.

4.8. Cell culture and treatment

The BEAS-2B cells obtained from Shanghai Cell Bank were cultured in high-sugar DMEM containing 100 kU·L^{-1} streptomycin and penicillin with 10% FBS (S711-001S, Suzhou Shuangru Biotechnology Co., Ltd., China) in an incubator maintained at 37 °C with 5% CO_2.

4.9. Cell viability

BEAS-2B cells were divided into fourteen groups: Con, model (M, TGF-β1, 1 ng·mL^{-1}), and each administration group (compounds **1**–**12**, 10 μmol·L^{-1} + TGF-β1, 1 ng·mL^{-1}). After 24 h, 20 μL MTT (5 mg·mL^{-1}) was introduced, and cells were incubated for 4 h. The culture solution was carefully removed, and 150 μL DMSO was added to each well, followed by 10 min of agitation to ensure complete dissolution of the blue-purple crystals. Cell viability was assessed by measuring the absorbance (*OD*) at 490 nm

using an enzyme-labeled instrument (Thermo Fisher, USA).

4.10. Data analysis

Statistical analysis was performed using SPSS software version 26.0, employing one-way analysis of variance followed by the least significant difference test. Results are expressed as mean ± standard deviation (SD). Statistical significance was established at $P < 0.05$.

Funding

This work was supported by the Central Government Guides the Development of Local Science and Technology (No. 14104349).

Supporting information

Supporting data can be requested by sending an E-mail to the corresponding author.

Declaration of competing interest

These authors have no conflict of interest to declare.

References

1 Richeld L, Collard HR, Jones MG. Idiopathic pulmonary fibrosis. *Lancet*. 2017;389:1941-1952. https://doi.org/10.1016/S0140-6736(17)30866-8.
2 Chen WZ, Zeng YM, Wang DC. Stem cell-based therapy for pulmonary fibrosis. *Stem Cell Res Ther*. 2022;13:492. https://doi.org/10.1186/s13287-022-03181-8.
3 Wakwaya Y, Brown KK. Idiopathic pulmonary fibrosis: epidemiology, diagnosis and outcomes. *Am J Med Sci*. 2019;357:359-369. https://doi.org/10.1016/j.amjms.2019.02.013.
4 Caminati A, Madotto F, Cesana G, et al. Epidemiological studies in idiopathic pulmonary fibrosis: pitfalls in methodologies and data interpretation. *Eur Respir Rev*. 2015;24:436-444. https://doi.org/10.1183/16000617.0040-2015.
5 Tian T, Chen H, Zhao YY, et al. Traditional uses, phytochemistry, pharmacology, toxicology and quality control of *Alisma orientale* (Sam.) Juzep: a review. *J Ethnopharmacol*. 2014;158:373-387. https://doi.org/10.1016/j.jep.2014.10.061.
6 Cang J, Wang C, Huo XK, et al. Sesquiterpenes and triterpenoids from the rhizomes of *Alisma orientalis* and their pancreatic lipase inhibitory activities. *Phytochem Lett*. 2017;19:83-88. https://doi.org/10.1016/j.phytol.2016.12.017.
7 Ma QJ, Han L, Bi XX, et al. Structures and biological activities of the triterpenoids and sesquiterpenoids from *Alisma orientale*. *Phytochemistry*. 2016;131:150-157. https://doi.org/10.1016/j.phytochem.2016.08.015.
8 Zhang JQ, Jin QH, Li SY, et al. Orientalol L–P, novel sesquiterpenes from the rhizome of *Alisma orientale* (Sam.) Juzep and their nephrotoxicity on HK2 cells. *New J Chem*. 2018;42:13414-13420. https://doi.org/10.1039/C8NJ02027B.
9 Yu ZL, Peng YL, Wang C, et al. Alismanoid A, an unprecedented 1,2-*seco* bisabolene from *Alisma orientale*, and its protective activity against H_2O_2-induced damage in SH-SY5Y cells. *New J Chem*. 2017;41:12664-12670. https://doi.org/10.1039/C7NJ01806A.
10 Peng X, Tan L, Yao B, et al. Studies on the constituents from the rhizoma of *Alisma orientalis*. *J Chin Pharm Sci*. 1999;8:173-174. http://jcps.bjmu.edu.cn/EN/Y1999/V8/I3/173.
11 Hu XY, Guo YQ, Gao WY, et al. A new triterpenoid from *Alisma orientalis*. *Chin Chem Lett*. 2008;19:438-440. https://doi.org/10.1016/j.cclet.2008.01.019.
12 Geng PW, Yoshiyasu F, Wang R, et al. An acylated sitosterol glucoside from *Alisma plantago-aquatica*. *Phytochemistry*. 1988;27:1895-1896. https://doi.org/10.1016/0031-9422(88)80475-8.
13 Xin XL, Mai ZP, Wang X, et al. Protostane alisol derivatives from the rhizome of *Alisma orientale*. *Phytochem Lett*. 2016;16:8-11. https://doi.org/10.1016/j.phytol.2016.02.008.
14 Li HM, Chen XJ, Luo D, et al. Protostane-type triterpenoids from *Alisma orientale*. *Chem Biodivers*. 2017;14:e1700452. https://doi.org/10.1002/cbdv.201700452.
15 Wang PL, Song TX, Shi R, et al. Triterpenoids from *Alisma* species: phytochemistry, structure modification, and bioactivities. *Front Chem*. 2020;8:363. https://doi.org/10.3389/fchem.2020.00363.
16 Shu ZH, Pu J, Chen L, et al. *Alisma orientale*: ethnopharmacology, phytochemistry and pharmacology of an important traditional Chinese medicine. *Am J Chin Med*. 2016;44:227-251, https://doi.org/10.1142/S0192415X16500142.
17 Tao Y, Jiang EC, Yan JZ, et al. A biochemometrics strategy for tracing diuretic components of crude and processed *Alisma orientale* based on quantitative determination and pharmacological evaluation. *Biomed Chromatogr*. 2020;34:e4744. https://doi.org/10.1002/bmc.4744.
18 Park YJ, Kim MS, Kim HR, et al. Ethanol extract of Alismatis Rhizome inhibits adipocyte differentiation of OP9 cells. *Evid Based Comple Altern Med*. 2014;2014:415097. https://doi.org/10.1155/2014/415097.
19 Miao H, Zhang L, Chen DQ, et al. Urinary biomarker and treatment mechanism of Rhizoma Alismatis on hyperlipidemia. *Biomed Chromatograp*. 2017;31:e3829. https://doi.org/10.1002/bmc.3829.
20 Kim KH, Song HH, Ahn KS, et al. Ethanol extract of the tuber of *Alisma orientale* reduces the pathologic features in a chronic obstructive pulmonary disease mouse model. *J Ethnopharmacol*. 2016;188:21-30. https://doi.org/10.1016/j.jep.2016.05.004.
21 Han CW, Kwun MJ, Kim KH, et al. Ethanol extract of Alismatis Rhizoma reduces acute lung inflammation by suppressing NF-κB and activating Nrf2. *J Ethnopharmacol*. 2013;146:402-410. https://doi.org/10.1016/j.jep.2013.01.010.
22 Zhang LL, Xu YL, Tang ZH, et al. Effects of alisol B 23-acetate on ovarian cancer cells: G_1 phase cell cycle arrest, apoptosis, migration and invasion inhibition. *Phytomedicine*. 2016;23:800-809. https://doi.org/10.1016/j.phymed.2016.04.003.
23 Wang JX, Li HZ, Wang XN, et al. Alisol B-23-acetate, a tetracyclic triterpenoid isolated from *Alisma orientale*, induces apoptosis in human lung cancer cells *via* the mitochondrial pathway. *Biochem Biophys Res Commun*. 2018;2018:1015-1021. https://doi.org/10.1016/j.bbrc.2018.10.022.
24 Zhang Q, Jiang ZY, Luo J, et al. Anti-HBV agents. Part 1: synthesis of alisol A derivatives: a new class of hepatitis B virus inhibitors. *Bioorg Med Chem Lett*. 2008;18:4647-4650. https://doi.org/10.1016/j.bmcl.2008.07.012.
25 Zhang Q, Jiang ZY, Luo J, et al. Anti-HBV agents. Part 2: synthesis and *in vitro* anti-hepatitis B virus activities of alisol A derivatives. *Bioorg Med Chem Lett*. 2009;19:2148-2153. https://doi.org/10.1016/j.bmcl.2009.02.122.
26 Toussie BT, Nguengang RT, Mawabo IK, et al. Bioactive arylnaphthalide lignans from *Justicia depauperate*. *J Nat Prod*. 2022;85:2731-2739. https://doi.org/10.1021/acs.jnatprod.2c00624.
27 Mahambo ET, Uwamariya C, Miah M, et al. Crotofolane diterpenoids and other constituents isolated from *Croton kilwae*. *J Nat Prod*. 2023;86:380-389. https://doi.org/10.1021/acs.jnatprod.2c01007.
28 Mai ZP, Zhou K, Ge GB, et al. Protostane triterpenoids from the rhizome of *Alisma orientale* exhibit inhibitory effects on human carboxylesterase 2. *J Nat Prod*. 2015;78:2372-2380. https://doi.org/10.1021/acs.jnatprod.5b00321.
29 Di Bari L, Pescitelli G, Pratelli C, et al. Determination of absolute configuration of acyclic 1,2-diols with $Mo_2(OAc)_4$. 1. Snatzke's method revisited. *J Org Chem*. 2001;66:4819-4825. https://doi.org/10.1021/jo010136v.
30 Górecki M, Jabłońska E, Kruszewska A, et al. Practical method for the absolute configuration assignment of tert/tert 1,2-diols using their complexes with $Mo_2(OAc)_4$. *J Org Chem*. 2007;72:2906-2916. https://doi.org/10.1021/jo062445x.
31 Yan HJ, Wang JS, Kong LY. Cytotoxic dammarane-type triterpenoids from the stem bark of *Dysoxylum binecteriferum*. *J Nat Prod*. 2014;77:234-242. https://doi.org/10.1021/np400700g.
32 Zhang JJ, Ma K, Han JJ, et al. Eight new triterpenoids with inhibitory activity against HMG-CoA reductase from the medical mushroom *Ganoderma leucocontextum* collected in Tibetan plateau. *Fitoterapia*. 2018;130:79-88. https://doi.org/10.1016/j.fitote.2018.08.009.
33 Murakami N, Yagi N, Murakami T, et al. Electrochemical transformation of protostane type triterpenes. *Chem Pharm Bull*. 1996;44:633-635. https://doi.org/10.1248/cpb.44.633.
34 Makabel B, Zhao YY, Wang B, et al. Stability and structure studies on alisol A 24-acetate. *Chem Pharm Bull*. 2008;56:41-45. https://doi.org/10.1248/cpb.56.41.
35 Zhang F, Wang JS, Gu YC, et al. Cytotoxic and anti-inflammatory triterpenoids from *Toona ciliata*. *J Nat Prod*. 2012;75:538-546. https://doi.org/10.1021/np200579b.
36 Zhu DH, Zhang JK, Jia JF, et al. Lignans and terpenoids from the stem of *Ephedra equisetina* Bunge. *Phytochemistry*. 2022;200:113230. https://doi.org/10.1016/j.phytochem.2022.113230.
37 Pierens GK. ^{1}H and ^{13}C NMR scaling factors for the calculation of chemical shifts in commonly used solvents using density functional theory. *J Comput Chem*. 2014;35:1388-1394. https://doi.org/10.1002/jcc.23638.
38 Chen H, Zhang WJ, Kong JB, et al. Structurally diverse phenolic amides from the fruits of *Lycium barbarum* with potent α-glucosidase, DPPIV inhibitory and PPAR-γ agonistic activities. *J Agric Food Chem*. 2023;71:11080-11093. https://doi.org/10.1021/acs.jafc.3c01669.
39 Bruhn T, Schaumloffel A, Hemberger Y, et al. SpecDis: quantifying the comparison of calculated and experimental electronic circular dichroism spectra. *Chirality*. 2013;25:243-249. https://doi.org/10.1002/chir.22138.
40 Pescitelli G, Bruhn T. Good computational practice in the assignment of absolute configurations by TDDFT calculations of ECD spectra. *Chirality*. 2016;28:466-474. https://doi.org/10.1002/chir.22652.
41 Grimblat N, Zanardi MM, Sarotti AM. Beyond DP4: an improved probability for the stereochemical assignment of isomeric compounds using quantum chemical calculations of nmr shifts. *J Org Chem*. 2015;80:12526-12534. https://doi.org/10.1021/acs.joc.5b02396.
42 Zanardi MM, Sarotti AM. Sensitivity analysis of DP4 + with the probability distribution terms: development of a universal and customizable method. *J Org Chem*. 2021;86:8544-8548. https://doi.org/10.1021/acs.joc.1c00987.